Chapter 5

A dress to impress: ordered melanin layers produce seductively shiny occipital feathers of the bird of paradise Lawes's parotia

Abstract

The male Lawes's parotia, a bird of paradise, uses the highly directional reflection of the occipital feathers in its courtship display. This brilliant-silvery plumage has a broad-band spectrum, but -unusually for structural plumage coloration- the reflectance peak wavelength is at ~1.3 μm, in the near-infrared. As in other birds, the structural coloration is produced by ordered melanin pigmentation to produce a multilayer interference reflector. The parotia's feather barbules contain 6-7 layers of densely packed melanin rodlets (diameter ~0.25 μm, length ~2 μm), which are separated by ~0.2 μm thick keratin layers. The high degree of order of these barbules allows us to apply a newly developed Jamin-Lebedeff interference microscopic method to make the first accurate, wavelength-dependent refractive index measurements of melanin in avian plumage. By taking into account the strong wavelength-dependent absorption of melanin, we have modelled the feather reflectance with optical multilayer theory. The model predictions agree well with direct measurements of the spectral, directional and polarization characteristics of the reflected light. The melanin refractive index obtained can be widely applied to structural coloration of animal integuments, especially avian plumage.

* Submitted.

Introduction

In many animal integuments melanins produce dull red, brown and black colours, but its high refractive index means that with nanoscale order melanin in a matrix of vertebrate keratin or arthropod chitin can produce structural colours [1-4]. The magnificent displays of birds of paradise exemplify how the basic bird feather barbule can be modified to achieve a range of visual effects through structural coloration. Thus, in Lawes's parotia (*Parotia lawesii*) the breast feather barbules have a boomerang-shaped cross-section, which produces three directional-coloured reflectors [5]. This unique structure allows the breast colour to switch sharply between yellow, blue and black as the bird moves, presumably to impress potential mates [6-8]. Here we investigate the parotia's occipital feathers (i.e. from the dorsal upper neck), which produce a shiny, silvery patch, that visually appear more like fish-scales than feathers (figure 1a,b). Compared to the breast feathers the occipital feathers are less colourful, having a broad band spectrum with peak wavelength in the near-infrared at about 1300 nm, but instead rely for their effect on highly directional reflection.

The directional reflection implies a highly ordered structure, and anatomy shows a multilayer of melanin rodlets in the occipital feather barbules. Here we seek to account quantitatively for the way in which the feather structure produces the structural coloration. The principles of reflecting multilayers are established [9], but understanding melanin-based structural coloration requires the refractive index value of melanin, which is poorly known. Melanin is a strongly absorbing pigment, and hence has a complex refractive index, in which the real component corresponds to the familiar refractive index of non-absorbing matter and the imaginary part accounts for light absorption. For melanin granules in pigeon feathers, Schmidt [1] found that the real part of the refractive index approaches that of ruby and sapphire (i.e. 1.76-1.77). However, work on structural coloration has generally used the round figure of 2.0 [2,9-12], originally assumed for hummingbird feathers [13]. Recent studies on insects indicate that this value is much too high, however [14-15]. An estimate derived by modelling the structural coloration of a beetle (*Chrysochroa fulgidissima*) predicts that the real part of the melanin refractive index oscillates between ~1.60 and ~1.72 [16].

The highly ordered structure of the parotia's occipital feathers allows us to measure directly the complex refractive index of feather melanin with a new interference method [17-18]. The data confirm previous estimates of the refractive index of insect melanin and moreover allow the first detailed optical analysis of melanin-based structural coloration in feather barbules. More generally, the optical properties of melanin can now be incorporated into any model of structural coloration, substantially improving the link between the nanostructure and optical properties of biological materials.

Results

Feather colour and structure

Lawes's parotia has a silvery-bluish occipital patch (figure 1a,b), which is produced by a reflective structure on the tip of each feather. The remainder of the feather, which is not normally visible, has brown melanin-pigmentation (figure 1c). In the main distal part of the

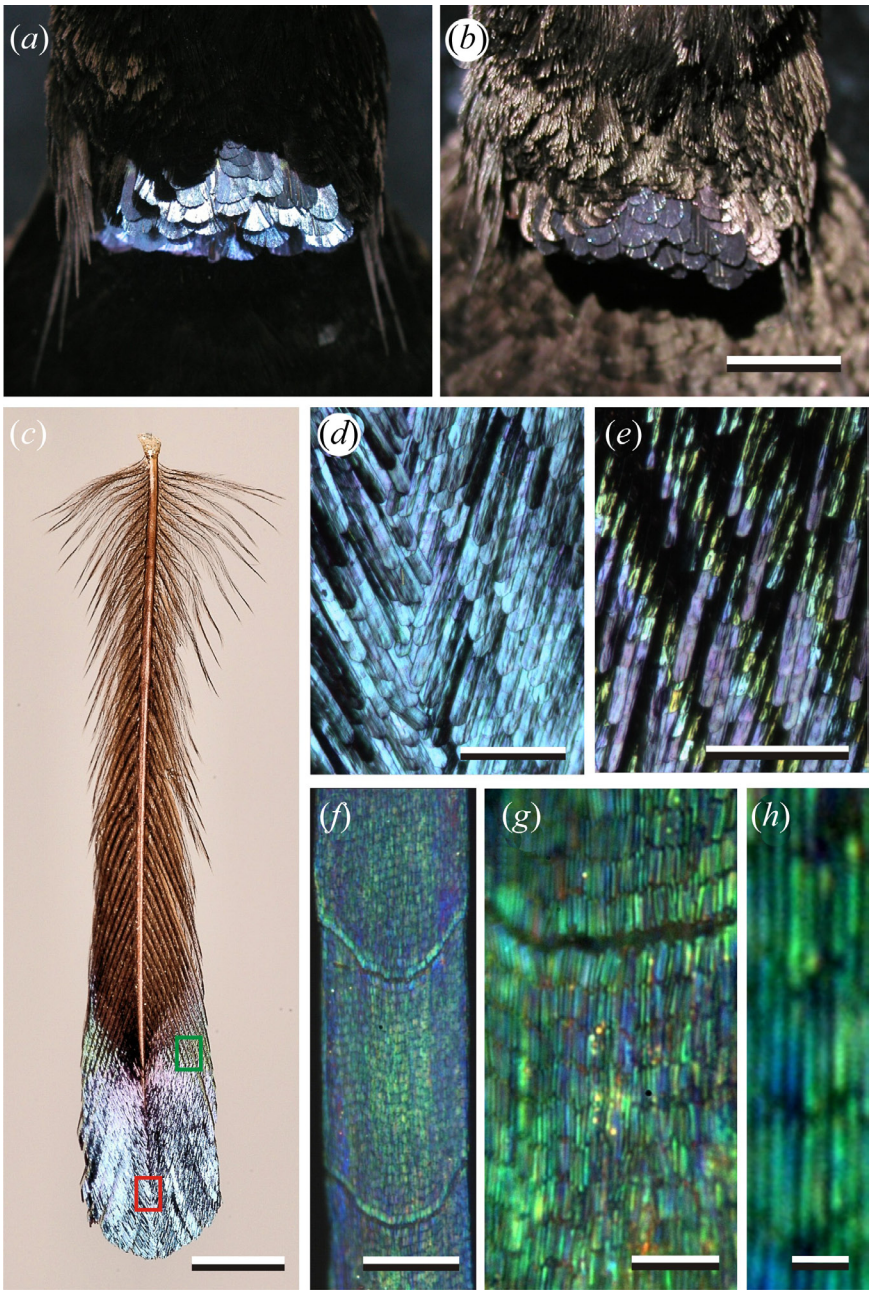

Figure 1. The occipital feathers of Lawes's parotia. (*a*) The occipital area illuminated with a narrow-aperture light beam and photographed from the mirror angle to show the reflective occipital feathers. (*b*) Slight rotation sharply reduces the silvery reflection. (*c*) A single occipital feather, showing silvery-reflective distal barbules and brown proximal barbules, which *in situ* are exposed and covered by other feathers, respectively. The red and green rectangles correspond to *d* and *e*. (*d*) With epi-illumination the distal barbules segments are bluish silvery. (*e*) The transition area, between the distal and proximal feather parts. The barbule segments here have a variable colour, from purple to greenish. (*f*) A single barbule immersed in a fluid with refractive index 1.63 (at 589 nm) showing bands of melanin rodlets (epi-illumination). (*g*) At higher magnification individual rodlets can be discerned. (*h*) Close-up view showing the single melanin rodlets, parallel arranged in bands. Scale-bars: (*a*,*b*) 1 cm; (*c*) 2 mm; (*d*,*e*) 200 μm; (*f*) 20 μm; (*g*) 5 μm; (*h*) 1 μm.

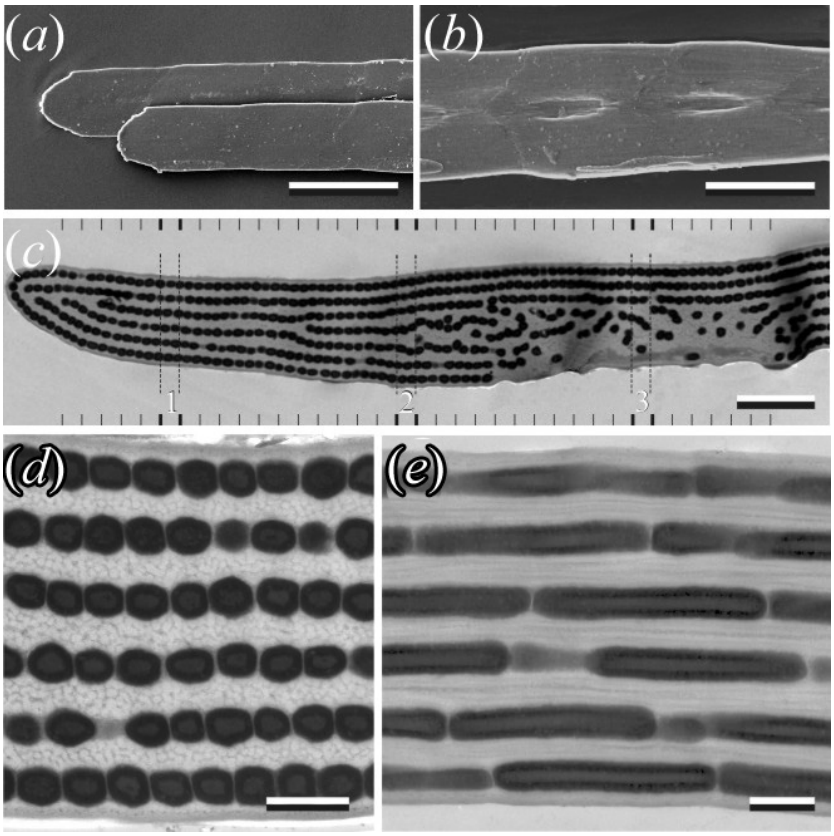

Figure 2. Scanning and transmission electron microscopy of occipital feather barbules. (*a*) Two barbules viewed from the upper side, showing a flat and smooth surface. (*b*) A barbule viewed at the underside, showing a slight depression at the centre of each cell. (*c*) A cross-section, revealing ordered layers of rodlets. The order is distorted in a central area at the underside. The short vertical bars indicate 36 vertical lanes, 0.5 μm wide, for which reflectance, transmittance and absorptance spectra were calculated. For the three lanes flanked by bold bars (numbered 1, 2, 3, and marked by dotted border lines) calculated refractive index profiles and spectra are given in figure 5. (*d*) Cross-section of the rodlets, diameter of ~250 nm, showing a ~60 nm thick cladding with a higher electron density than the core. (*e*) Longitudinal section of the rodlets. Bars: (*a*) 50 μm; (*b*) 25 μm; (*c*) 2 μm; (*d*,*e*) 0.5 μm.

feather the barbule cells vary little in colour (figure 1d), but in the transition area between the silvery and brown regions the cell colour can abruptly change from violet to green (figure 1e). Light microscopy of the distal barbules, immersed in a high refractive index medium (n = 1.63 at 589 nm), reveals a fine cellular structure in the sub-micrometre range, with bands of slender, parallel rodlets ~2.0 μm long and ~0.25 μm wide (figure 1f-h). An obvious hypothesis is that this fine-structure produces the feathers' reflectivity.

Scanning electron microscopy demonstrated that the barbule upper surface is smooth, except for slight ridges at the cell boundaries (figure 2a), but the underside has an indentation in the centre of each cell (figure 2b). In transverse TEM cross-sections the barbule has a striking internal organization, with 6 - 7 layers of closely apposed round particles (figure 2c,d). At the barbule centre, in the area of indentation (figure 2b), the number of layers is reduced and the parallel layering is distorted (figure 2c). The indentation and the layer distortion are probably the remains of the cell nucleus [1]. Longitudinal cross-sections of the barbule

(figure 2e) confirm the presence (figure 1h) of layers of slender rodlets, length ~2 μm and diameter ~0.25 μm. Each rodlet comprises a cladding (thickness ~60 nm) surrounding a core with a slightly (<10%) lower electron density (figure 2d,e).

Barbule pigmentation

The barbules observed with transmitted light show that the pigmentation in the centre of each barbule cell is less than in the surrounding area (compare figure 2c with figure 3a, upper inset). Transmittance spectra, measured from the two regions with a microspectrophotometer (figure 3a), are characteristic for melanin pigmentation, which is less dense in the centre. Transmittance spectra of the occipital feather barbules, like those of figure 3a, converted to absorbance spectra were well fitted by an exponential function $D = D_0 \exp(-\lambda/\lambda_m)$, with $\lambda_m = 155 \pm 8$ nm. The latter value indicates that the pigment is mostly eumelanin, because the absorbance spectra of eumelanin and pheomelanin, which often coexist in bird feathers [21], are described by exponential functions with $\lambda_m = 115$ nm and $\lambda_m = 175$ nm, respectively [17].

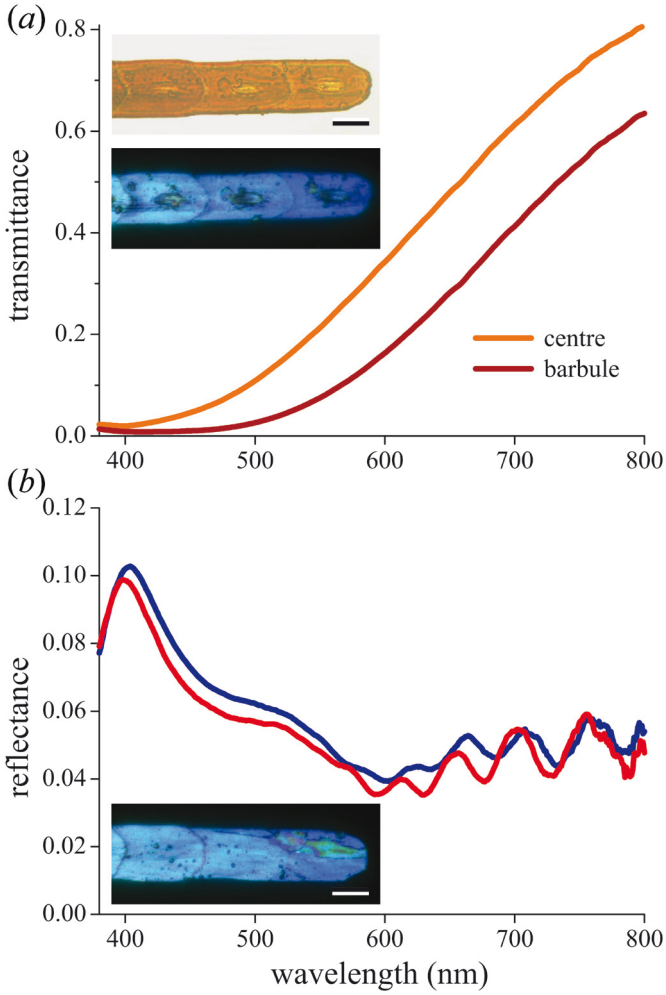

Figure 3. Reflectance and transmittance spectra of small barbule areas. (*a*) Transmittance spectra obtained by microspectrophotometry, measured from the centre of a barbule and from the surrounding area. Inset: above, the barbule observed with transmitted light; below, epi-illumination from the underside; bar 20 μm. (*b*) Reflectance spectra measured from small barbule areas (5 μm diameter, upper surface) showing oscillations reminiscent of thin film interference. Inset: the same barbule as the inset of *a* observed with epi-illumination from the upper side; bar: 20 μm.

Reflectance spectra of the two measured barbule areas (figure 3b) peak in the blue-violet wavelength range (c.f. figure 1), but also show oscillations in the long-wavelength range that are characteristic of thin-film interference. Evaluation of the oscillation periods (for procedure, see [22]) and assuming an average refractive index of the barbule of 1.6 yielded a thin film thicknesses of approximately 3.0 μm; which is indeed about the thickness of a barbule (figure 2c). In other words, the barbule behaves in part as a thin film reflector. Yet, the barbule internal structure, with the highly ordered melanin layers that have a strongly wavelength-dependent absorption, must contribute to the reflectance.

We can assess the contribution of the melanin multilayer by multilayer modelling, but this requires knowledge of the refractive index values of the melanin and keratin layers. We achieved this by first measuring the effective refractive index of the feather barbule, that is in the main barbule area as well as in the barbule centre, at a number of wavelengths, using Jamin-Lebedeff interference microscopy (for details, see chapter 3). The resulting refractive index values were fitted with the Cauchy equation: $n(\lambda) = A + B/\lambda^2$ (figure 4). This yielded for the main barbule area Cauchy parameters $A = 1.590 \pm 0.001$ and $B = (1.48 \pm 0.07)\cdot 10^4$ nm^2, and for the centre $A = 1.572 \pm 0.002$ and $B = (1.17 \pm 0.01)\cdot 10^4$ nm^2.

The derived refractive index values are weighted sums of the refractive indices of the melanin and keratin constituents. For the keratin of white goose feathers we found Cauchy parameters $A = 1.532 \pm 0.001$ and $B = (5.89 \pm 0.02)\cdot 10^3$ nm^2 ([19]; figure 4). Assuming that the keratins of bird of paradise and goose feathers are alike, this means that the Cauchy parameters for the barbule area and keratin differ by $\Delta A = 0.058 \pm 0.002$ and $\Delta B = (0.89 \pm 0.09)\cdot 10^4$ nm^2; for the centre area the differences are $\Delta A = 0.040 \pm 0.003$ and $\Delta B = (0.58 \pm 0.03)\cdot 10^4$ nm^2. The increase in the effective refractive index in the centre with respect to keratin thus is about 2/3 of the refractive index increase in the main barbule area. This agrees with the anatomical data, showing an approximately 2/3 reduction in the concentration of electron dense particles in the centre area (figure 2c).

To estimate the refractive index of melanin we used the measured barbule refractive index to derive a refractive index profile. To this end we divided the barbule cross-section shown in Figure 2c into 0.5 μm wide lanes, and converted the density values into refractive index values (see Methods). Figure 5a presents the real part of the refractive index profiles, for 500 nm light, derived for the three lanes numbered 1-3 in figure 2c. The refractive index oscillates more or less sinusoidally, with a periodicity determined by the layering in the lanes. For wavelengths other than 500 nm the modulations are similar, but with increasing wavelength the modulation slightly decreases due to dispersion. This slight decrease holds for the real part of the refractive index, but the imaginary part is strongly wavelength-dependent, because melanin absorption increases strongly with decreasing wavelength. The extreme refractive index value is about 1.79 (at 500 nm; figure 5a), which accordingly represents the value for concentrated melanin. The Cauchy parameters for the corresponding melanin refractive index are $A = 1.677$ and $B = 2.81\cdot 10^4$ nm^2; Figure 4 (upper curve) gives the spectral dependence.

Multilayer modelling of the barbule

To understand the occipital feather coloration, we implemented the refractive index profiles (figure 5a) in a multilayer model [16], which yielded the reflectance, transmittance and

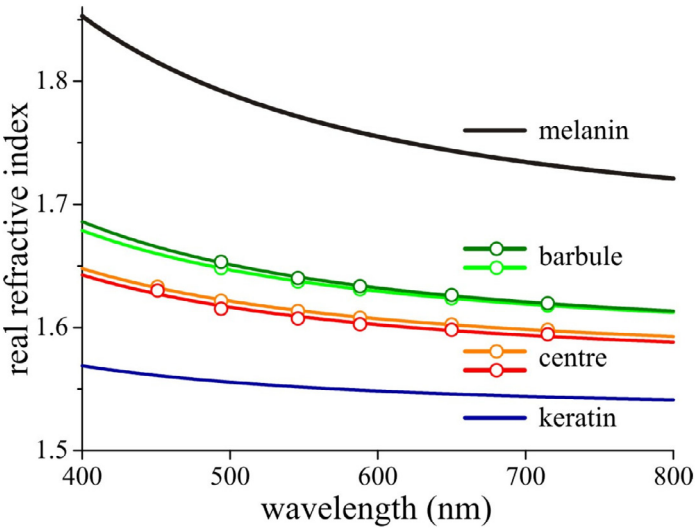

Figure 4. Real part of the refractive index of barbule and centre areas as a function of wavelength, derived from Jamin-Lebedeff interference microscopy, together with Cauchy function fits. The melanin refractive index spectrum was derived from these data and the bird (white goose) keratin spectrum.

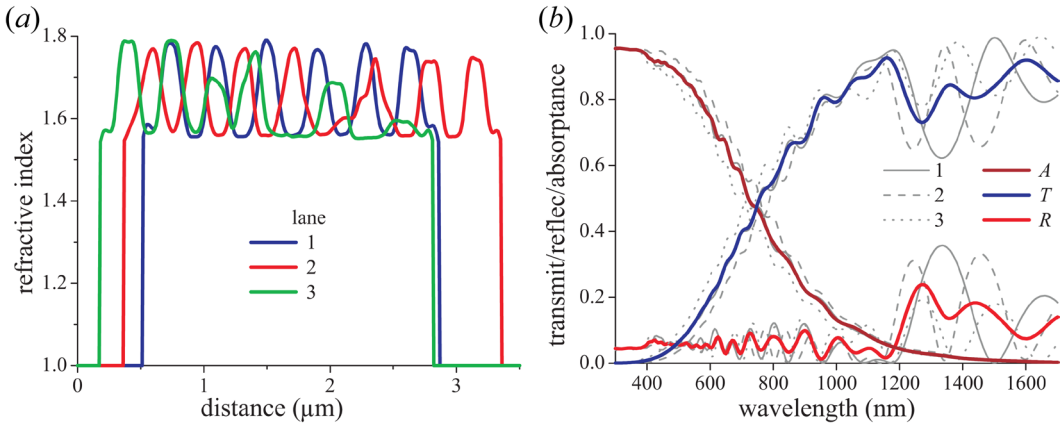

Figure 5. Refractive index gradients and their spectral consequences. (*a*) The real part of the refractive index at 500 nm for the three, 0.5 μm-wide lanes numbered 1, 2 and 3 in figure 2c. (*b*) Absorptance (*A*), transmittance (*T*) and reflectance (*R*) spectra calculated with a multilayer model for lanes 1-3 (grey curves) and the averaged spectra (coloured curves).

absorptance of the three lanes of the feather (figure 5b; solid, dashed and dotted grey curves for lanes 1-3). The model calculations predict that the *absolute* reflectance, *R*, in the visible wavelength range is meagre, less than 10%, but the reflectance peaks in the infrared, in the wavelength range 1200-1600 nm, with maximal values of ~30%. The peak wavelengths for the different lanes vary, clearly due to differences in the refractive index periodicity. The absorptance, *A*, is very low in the infrared, because of the low absorption of melanin there; thus the transmittance, $T = 1\text{-}R\text{-}A$, mirrors the reflectance in the long-wavelength range. Notably, all of the modelled reflectance spectra have strong, periodic oscillations in the 600-1000 nm wavelength range. We already concluded above that the oscillations are due to the total barbule thickness, acting as a thin film. As one would expect, the averaged spectra for the three lanes yield smoothed spectra (figure 5b, coloured curves; for similar effects see [23]).

Angle-dependent reflection of the distal barbules

To investigate the angle-dependence of the reflectance spectrum of the occipital feathers we extended the reflectance calculations of figure 5 to 36 lanes (figure 2c). For each lane we calculated the reflectance as a function of the angle of light incidence, and then averaged the reflectance spectra. The calculations were performed for both TE- and TM-polarized light (figure 6a,c). As expected for a multilayer, with increasing angle of incidence, the infrared peak shifted to shorter wavelengths for both TE-polarized light and TM-polarized light. The peak height increased for TE-polarized light and decreased for TM-polarized light.

To verify the validity of the calculations we measured the angle-dependent reflectance of the occipital feather in both the visible and infrared wavelength range with a setup consisting of two rotatable optical fibres (figure 6b,d). The illumination spot, with a spot diameter of ~4 mm, approximately covered the entire shiny part of the feather. The illumination fibre angle was varied in 10° steps and at each step the detection fibre was moved until a maximal signal was obtained. This position always closely approximated the mirror angle. Of course, the experimental spectra do not precisely match the calculated spectra, but the overall behaviour is very similar (figure 6).

Directional reflectance

Both the angle-dependent reflectance measurements (figure 1a,b) and the laminar organization of the melanin rodlets in the occipital feather (figure 2) were consistent with the mirror-like appearance. We used an imaging scatterometer to measure directly the directionality of the reflected light [16,20]. When illuminated with a narrow-aperture, white-light beam the feather had a narrow-aperture reflection. As for any flat mirror, rotation of the feather deflected the reflected beam by twice the angle of rotation (figure 7a).

For mirror-like objects, hemispherical illumination, that is light incident from all angles above the object, can be applied to document the angle-dependent reflection properties in a single image (figure 7b). With unpolarized light, the colour of the reflected light changed from blue through violet to white with an increase of the reflection angle (figure 7b). The latter is due to the fact that for very large angles of incidence the reflectance at any surface and multilayered structure approaches 100% for all wavelengths [16,24]. Upon adding a vertical polarizer a reflectance minimum for TM-polarized light emerged at the Brewster angle of ~60° (the dark spot at about +60º and -60º in the vertical plane, figure 7c; compare figure 6b,d). At angles larger than the Brewster angle the TM-reflectance increases again. The reflectance behaviour for TE-polarized light (horizontal plane, figure 7c) resembles that for unpolarised light (figure 7b), showing that in the latter case TE-polarised light dominates.

Discussion

As in other birds [2] the barbules of the occipital feathers of Lawes's parotia contain alternating layers of melanin rodlets and keratin, but here the exceptionally orderly structure gives a silvery appearance, which is not seen in any other feather. This order permitted the

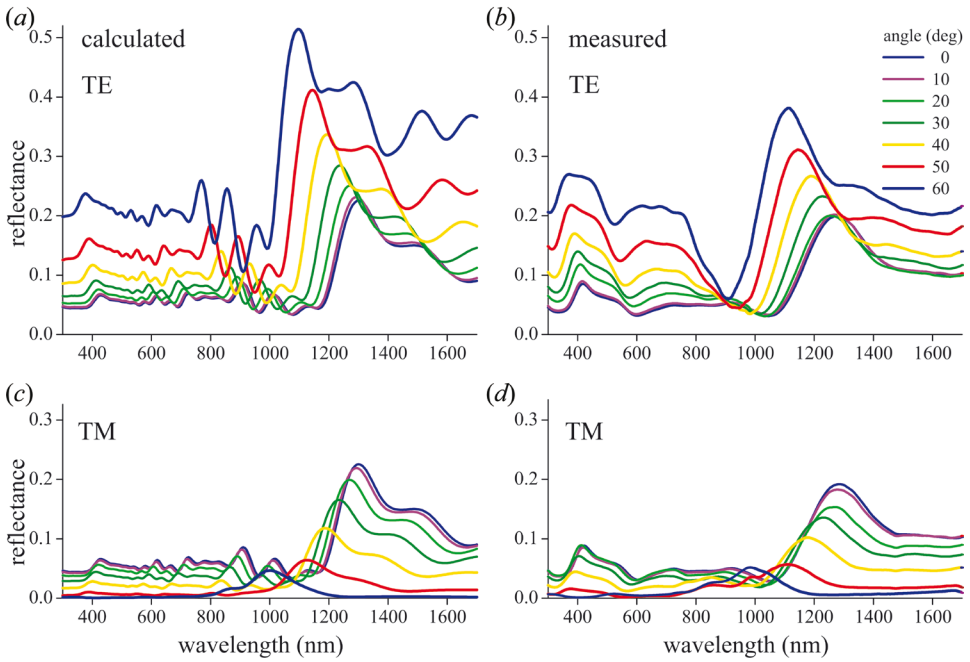

Figure 6. Angle-dependent reflectance spectra. (*a*) Averaged spectra for TE-polarized light, with angles of incidence from 0º to 60º, of the reflectance spectra calculated for 36 lanes of the transmission electron micrograph of figure 2c, using the refractive index values of figure 4c. (*b*) Experimental reflectance spectra for TE-polarized light. (*c*) As *a* for TM-polarized light. (*d*) As *b* for TM-polarized light.

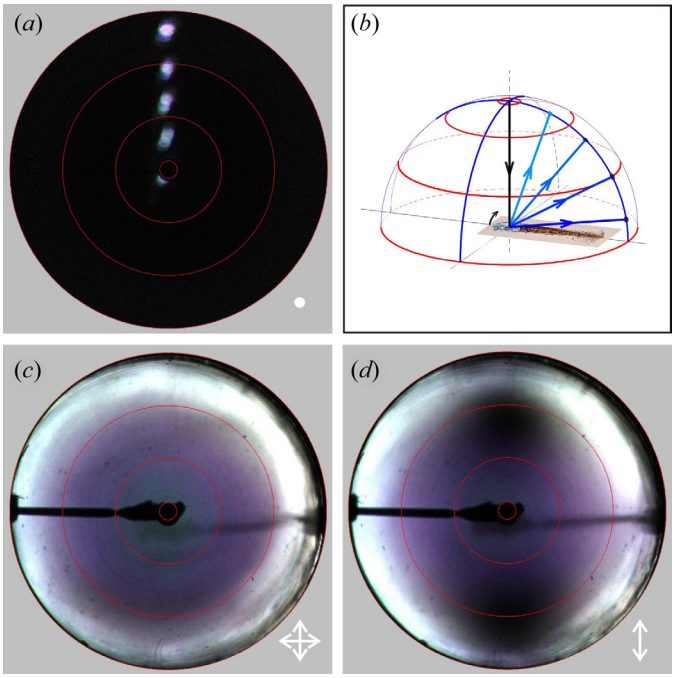

Figure 7. Imaging scatterometry of an occipital feather tip. (*a*) Illumination with a narrow-aperture (~5º) light beam yielded a similarly narrow-aperture reflected beam. Rotating the feather from the normal position in steps of 10º displaced the reflection spots in steps of 20º, as expected for a mirror-like surface, as illustrated in the diagram of panel *b* (see figure 1c). (*c*) Scatter pattern of the feather oriented normal to the central axis, illuminated with a wide aperture (180º) beam of unpolarized light (indicated by the crossed arrows). (*d*) Scatter pattern for the same wide aperture beam but with vertically polarized light (indicated by the vertical arrow). The reflection of TM-polarized light becomes minimal at Brewster's angle (dark spots around -60º and +60º at the vertical axis).

first accurate measurement of the melanin refractive index in feathers, and hence accurate modelling of their structural coloration.

The refractive index of melanin in feathers has been a matter of conjecture for several decades. For the pigeon *Columba trocaz*, whose barbule cells contain melanin granules and air spaces in a keratin matrix, application of a series of immersion fluids led Schmidt [1] to conclude that the granule refractive index exceeds 1.739 (n_D of methylene iodide), approximates 1.76-1.77 (ruby and sapphire), and is less than 2.42 (diamond). Subsequent studies have, for convenience, assumed a value 2.0 for the melanin refractive index (e.g. [2,9-12]). We show here that the real part of the refractive index of the melanin layers is $\leq$ 1.8 in the visible wavelength range (figure 5a).

The barbule as a multilayer and a thin film

The barbule acts as a multilayer interference reflector because of a refractive index contrast between the melanin and keratin layers [9,25,26]. Generally, when a multilayer comprises layers with alternating thicknesses d_l and d_h and (real parts of the) refractive indices n_l and n_h, the reflectance peak wavelength for normal illumination is $\lambda_{max} = 2(n_l d_l + n_h d_h)$ [9,26]. In the occipital feather barbules the thicknesses of the melanin and keratin layers are $d_l \approx d_h \approx 200$ nm (figure 2), with $n_l \approx 1.55$ and $n_h \approx 1.80$. It thus follows, somewhat surprisingly, that $\lambda_{max} \approx 1300$ nm, in the infrared, and satisfactorily, direct measurement confirms this estimate (figure 6). Within the visible wavelength range, the barbule reflectance is broad-band, slightly peaking at short wavelengths. Spectral oscillations in the red to far-red range seen with a small measurement spot (figure 3) are due to thin-film interference effects attributable to the full thickness of the barbule. With large-field measurement, the oscillations are smoothed (figure 6b,d), because barbule thickness varies over a large area (figures 2, 6).

Angle- and polarization-dependent reflection

The angle-dependent reflectance measurements yielded spectra that corresponded well with calculated spectra for both TE- and TM-polarized light. A perfect correspondence cannot be expected, because the calculations were for a TEM cross-section of part of a single barbule, while the experimental reflectance spectra were from an intact feather, containing several barbules, which are certainly not identical. Because the multilayer even within one and the same barbule is far from ideal, spectral calculations were performed for 0.5 μm wide lanes (figure 2c), and the resulting spectra were subsequently averaged (figure 6). The validity of this heuristic approach is underscored by the close correspondence of the peak wavelength in the infrared and the similar hypsochromic spectral shifts with increasing angle of light incidence in the calculations and the measurements. In fact, finite-difference time-domain (FDTD) modelling (see figure 8) yielded reflectance spectra matching those of the heuristic modelling. In conclusion, the combined reflectance measurements and modelling confirm the direct measurements of the melanin refractive index. The melanin data now can be used to model the reflectance properties of very differently structured feathers. In fact, implementing the melanin refractive index in an FDTD model of Lawes's multi-coloured breast feathers fully confirms the experimentally found three-directionality of the reflectance [5].

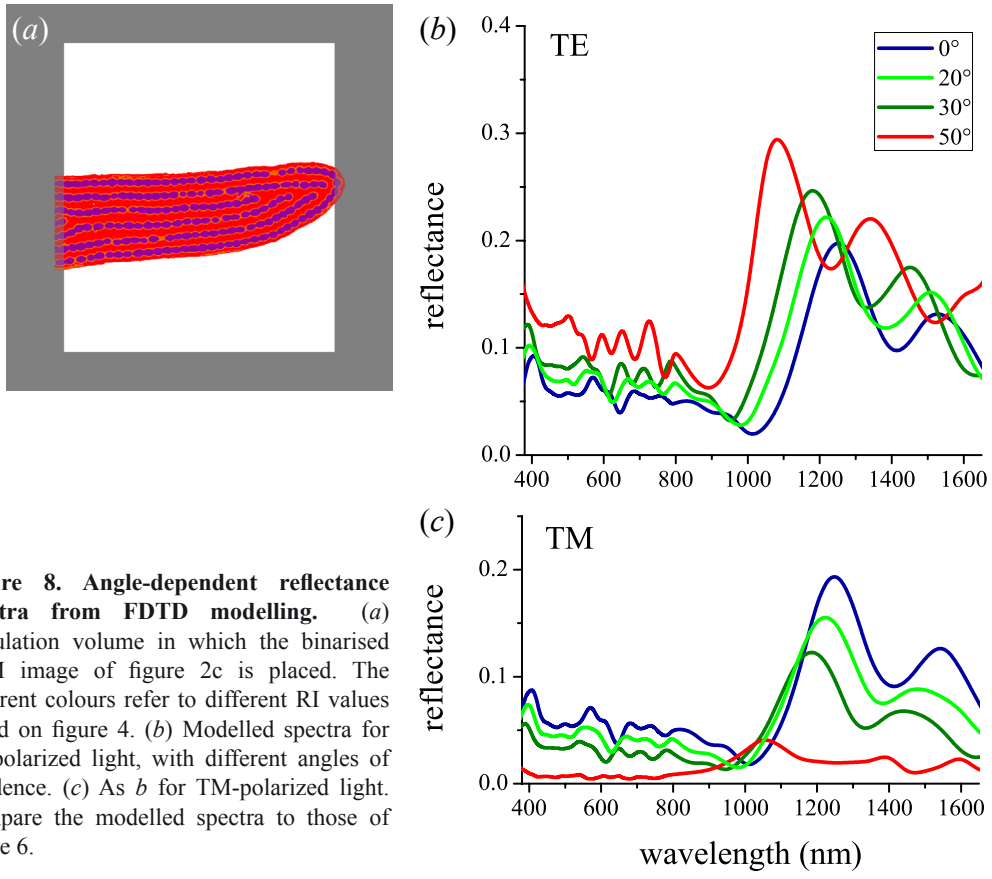

Figure 8. Angle-dependent reflectance spectra from FDTD modelling. (*a*) Simulation volume in which the binarised TEM image of figure 2c is placed. The different colours refer to different RI values based on figure 4. (*b*) Modelled spectra for TE-polarized light, with different angles of incidence. (*c*) As *b* for TM-polarized light. Compare the modelled spectra to those of figure 6.

In our previous study on the metallic green elytra of the Japanese Jewel Beetle *Chrysochroa fulgidissima* [16] we found angle- and polarization-dependences of reflectance spectra very similar to those presented here. Imaging scatterometry of the beetle elytra with wide-field, hemispherical illumination demonstrated that the reflection is polarized. The polarized reflection patterns might be used for intraspecific signalling, because beetles possess polarization vision. The occipital feather reflections are also polarized, but birds are unlikely to use the polarizing signals in this context [27].

Biological function of the specular occipital feathers

It seems likely that the very different optical and visual properties of the breast and occipital feathers have evolved for specific roles in signalling in Lawes's parotia courtship display [6-8]. The breast feathers reflect over a large spatial angle and produce dramatic colour changes [5] whereas the occipital feathers are silvery and highly directional. Both are surrounded by dense-black plumage to produce strong contrasts. Field observations on Wahnes's parotia (*Parotia wahnesi*), a close relative of Lawes's parotia, show that males, while on their forest-floor court, use the reflective occipital feather patch to reflect the shaft of light incident through the foliage towards the females, who observe the male's performance from an overhanging branch (E. Scholes and T. Laman, personal information).

Materials and Methods[1]

Occipital feathers and anatomy

Lawes's parotia occipital feathers (figure 1a,b) were from specimens in the Queensland Museum (Brisbane, Australia) and the Natural History Museum Naturalis (Leiden, the Netherlands). Single feathers were photographed with a Nikon D70 camera (figure 1c). Feather details were photographed with an Olympus SZX16 stereomicroscope and a Kappa DX40 (Kappa Optronics, Gleichen, Germany) camera (figure 1d,e). Single barbules immersed in a refractive index matching fluid (n = 1.63 at 589 nm) were photographed with a Zeiss (Oberkochen, Germany) Universal Microscope using Nikon Fluor 40/1.30 (figure 1f) and Zeiss 100/1.25 (figure 1g,h) oil objectives and the Kappa camera. The barbule surfaces were examined with a scanning electron microscope (Philips XL-30 ESEM; Eindhoven, the Netherlands), and their internal structure with transmission electron microscopy (figure 2).

Barbule refractive index and feather reflectance modelling

The refractive index of the barbules was measured with a new method based on Jamin-Lebedeff interference microscopy [18]. To determine the refractive index profile of the barbule, we divided the transmission electron micrograph (TEM) of figure 2c into 36 lanes, each 0.5 μm wide (indicated by the short vertical bars at the bottom and top of figure 2c), and recorded the average density of a 10 nm thick cross-section in each lane. The part of the barbule with the minimum density, D_{min}, was assumed to be pure keratin, and the refractive index was hence taken to be $n_k = 1.532+5.89\cdot10^3\lambda^{-2}$ [19]. In addition, the average density of the barbule, D_{av}, was determined. For each of the lanes, the density value in the jth 10 nm cross-section, D_j, was converted to a wavelength-dependent refractive index: $n_j = n_k + [\Delta n_{oR} + i n_{oI}][(D_j - D_{min})/(D_{av} - D_{min})]$, where $\Delta n_{oR} = n_{oR} - n_k$. In other words, the density $D_{av} - D_{min}$ was assumed to be proportional to the measured increase in the complex refractive index due to melanin, and the local density was scaled accordingly. The refractive index outside the barbule was set to 1.0 (air). A total path length of 3.5 μm was taken, slightly more than the full thickness of the barbule, which yielded 3500/10 = 350 refractive index values. These values were implemented in a multilayer program [16], which for each lane calculated the wavelength-dependent reflectance, R, and transmittance, T, as a function of incident angle and polarization; the absorptance followed from $A = 1-R-T$. The reflectance spectra calculated for the 36 lanes were averaged, and taken to be representative of the barbule reflectance spectrum (figure 6a,c).

References

1. Schmidt, W. J. 1952 Wie entstehen die Schillerfarben der Federn? *Naturwiss.* **39**, 313-318.
2. Durrer, H. 1977 Schillerfarben der Vogelfeder als Evolutionsproblem. *Denkschr. Schweiz. Naturforsch. Ges.* **91**, 1-126.
3. Prum, R. O. 2006 Anatomy, physics, and evolution of avian structural colors. In: *Bird Coloration, Vol. I, Mechanisms and Measurements* (eds. G. E. Hill & K. J. McGraw), pp. 295-353. Harvard University Press, Cambridge, Mass.
4. Nakamura, E., Yoshioka, S. & Kinoshita, S. 2008 Structural color of rock dove's neck feather. *J. Phys. Soc. Jpn* **77**, 124801.
5. Stavenga, D. G., Leertouwer, H. L., Marshall, N. J. & Osorio, D. 2010 Dramatic colour changes in a bird of paradise caused by uniquely structured breast feather barbules. *Proc. R. Soc. B* **278**, 2098-2104.
6. Pruett-Jones, S. G. & Pruett-Jones, M. A. 1990 Sexual selection through female choice in Lawes' parotia, a lek-mating bird of paradise. *Evolution* **44**, 486-501.
7. Frith, C. B. & Beehler, B. M. 1998 *The birds of paradise*. Oxford University Press, Oxford.
8. Scholes, E. 2008 Structure and composition of the courtship phenotype in the bird of paradise *Parotia lawesii* (Aves: Paradisaeidae). *Zoology* **111**, 260-278.
9. Land, M. F. 1972 The physics and biology of animal reflectors. *Progr. Biophys.* **24**, 77-105.
10. Zi, J., Yu, X. D., Li, Y. Z., Hu, X. H., Xu, C., Wang, X. J., Liu, X. H. & Fu, R. T. 2003 Coloration strategies in peacock feathers. *Proc. Natl. Acad. Sci. USA* **100**, 12576-12578.
11. Brink, D. J. & van der Berg, N. G. 2004 Structural colours from the feathers of the bird *Bostrychia hagedash*. *J. Phys. D: Appl. Phys.* **37**, 813-818.

[1] Materials and Methods are presented in more detail in **Chapters 2** and **3.**

12. Shawkey, M. D., Hauber, M. E., Estep, L. K. & Hill, G. E. 2006 Evolutionary transitions and mechanisms of matte and iridescent plumage coloration in grackles and allies (Icteridae). *J. R. Soc. Interface* **3**, 777-786.
13. Greenewalt, C. H., Brandt, W. & Friel, D. D. 1960 The iridescent colors of hummingbird feathers. *Proc. Amer. Phil. Soc.* **104**, 249-253.
14. Noyes, J. A., Vukusic, P. & Hooper, I. R. 2007 Experimental method for reliably establishing the refractive index of buprestid beetle exocuticle. *Opt. Express* **15**, 4351-4358.
15. Yoshioka, S. & Kinoshita, S. 2011 Direct determination of the refractive index of natural multilayer systems. *Phys. Rev. E* **83**, 051917.
16. Stavenga, D. G., Wilts, B. D., Leertouwer, H. L. & Hariyama, T. 2011 Polarized iridescence of the multilayered elytra of the Japanese Jewel Beetle, *Chrysochroa fulgidissima*. *Phil. Trans. R. Soc. B* **366**, 709-723.
17. Stavenga, D. G., Leertouwer, H. L., Hariyama, T., De Raedt, H. A. & Wilts, B. D. 2012 Sexual dichromatism of the damselfly *Calopteryx japonica* caused by a melanin-chitin multilayer in the male wing veins. *PlosONE* **7**: e49743.
18. Stavenga, D. G., Leertouwer, H. L. & Wilts, B. D. 2013 Quantifying the refractive index dispersion of a pigmented biological tissue using Jamin-Lebedeff interference microscopy. *Light Sci. Appl.*, **in press**
19. Leertouwer, H. L., Wilts, B. D. & Stavenga, D. G. 2011 Refractive index and dispersion of butterfly scale chitin and bird feather keratin measured by interference microscopy. *Opt. Express* **19**, 24061-24066.
20. Stavenga, D. G., Leertouwer, H. L., Pirih, P. & Wehling, M. F. 2009 Imaging scatterometry of butterfly wing scales. *Opt. Express* **17**, 193-202.
21. McGraw, K. J. 2006 Mechanics of melanin-based coloration. In: *Bird coloration* (eds. G. E. Hill & K. J. McGraw), pp. 243-294. Harvard, Cambridge, Mass.
22. Stavenga, D. G., Tinbergen, J., Leertouwer, H. L. & Wilts, B. D. 2011 Kingfisher feathers - colouration by pigments, spongy nanostructures and thin films. *J. Exp. Biol.* **214**, 3960-3967.
23. Trzeciak, T. M., Wilts, B. D., Stavenga, D. G. & Vukusic, P. 2012 Variable multilayer reflection together with long-pass filtering pigment determines the wing coloration of papilionid butterflies of the *nireus* group. *Opt. Express* **20**, 8877-8890.
24. Wilts, B. D., Michielsen, K., Kuipers, J., De Raedt, H. & Stavenga, D. G. 2012 Brilliant camouflage: photonic crystals in the diamond weevil, *Entimus imperialis*. *Proc. R. Soc. B* **279**, 2524-2530.
25. Srinivasarao, M. 1999 Nano-optics in the biological world: Beetles, butterflies, birds and moths. *Chem. Rev.* **99**, 1935-1961.
26. Kinoshita, S. 2008 *Structural colors in the realm of nature*. World Scientific, Singapore.
27. Muheim, R. 2011 Behavioural and physiological mechanisms of polarized light sensitivity in birds. *Phil. Trans. R. Soc. B* **366**, 763-771.